Study on the Impact of C-Class Solar Flares on Low-Frequency Signal Propagation and Ionospheric Disturbances

Luxi Huang [1], Zhen Qi [2], Shaohua Shi [1,2], Yingming Chen [1], Fan Zhao [1,2], Xin Wang [1,2], Feng Zhu [1], Xiaohui Li [1,2] and Ping Feng [1,2,*]

[1] National Time Service Center, Chinese Academy of Sciences, Xi'an 710600, China; huangluxi@ntsc.ac.cn (L.H.); shishaohua@ntsc.ac.cn (S.S.); cym@ntsc.ac.cn (Y.C.); zhaofan@ntsc.ac.cn (F.Z.); wangx@ntsc.ac.cn (X.W.); zhufeng@ntsc.ac.cn (F.Z.); lixiaohui@ntsc.ac.cn (X.L.)

[2] University of Chinese Academy of Sciences, Beijing 100049, China; qizhen@ntsc.ac.cn

* Correspondence: pingfp@ntsc.ac.cn; Tel.: +86-029-8389-0489

Abstract: This work investigates the impact of C-class solar flare events (XRA) on ionospheric and low-frequency signal propagation by analyzing the maximum correlation lag time, correlation, and Granger causality between low-frequency time-code signal strength and XRA. The results show that within the lag interval of $(-5, 5)$ minutes, XRA exhibits the highest correlation and causality with signal strength, supporting the theory of a rapid ionospheric response and early warning to XRA. The correlation coefficient increases significantly with flare intensity, indicating that XRA has both linear and nonlinear dual effects on the disturbance of low-frequency signal propagation paths. Granger causality tests further confirm that XRA events have an immediate and sustained direct impact on signal strength. These findings provide a basis for understanding the disturbance mechanism of solar activity on the Earth's ionosphere and support the use of low-frequency signals in space weather forecasting.

1. Introduction

Solar flares release a large amount of X-ray radiation during their eruption, which directly affects the D and E layers of the ionosphere, significantly increasing electron density. These rapid changes typically occur within minutes and can lead to dramatic fluctuations in the propagation characteristics of low-frequency signals, manifested as sudden increases or decreases in signal strength. There is already a significant body of research on the disturbances in the ionosphere caused by solar storms and their impact on the propagation of low-frequency signals. Previous studies have shown that solar storms significantly impact the ionospheric characteristics and radio wave propagation across high, middle, and low-latitude regions. Solar storms typically affect the polar ionosphere by triggering magnetic storms and enhancing auroral activity. Hayes et al. (2021) demonstrated that during solar storms, the dramatic changes in electron density induced by solar radiation cause the ionospheric response in the polar regions to be most pronounced, with strong auroral phenomena and magnetic field disturbances [1]. In the middle-latitude regions, the ionospheric response to solar storms is more complex, manifesting as variations in electron density, particularly affecting high-frequency communication. Nishimoto et al. (2021) emphasized that changes in solar flares and X-ray radiation lead to rapid ionospheric variations in the middle latitudes, significantly influencing the propagation of both low-

and high-frequency signals [2]. Although the impact on the ionosphere in low-latitude regions is relatively less pronounced, it still results in fluctuations that affect global positioning systems (GPS) and satellite communication. Liu et al. (2011) noted that ionospheric disturbances in low-latitude regions, primarily manifested as changes in Total Electron Content (TEC), can cause short-term disruptions to satellite communications [3]. Additionally, Nayak and Yiğit (2018) pointed out that ionospheric variations in low-latitude areas can significantly degrade signal quality for high-precision navigation systems, such as GPS, during solar storms [4]. The transmitting station (Shangqiu) and receiving station (Xi'an) in this study are both located in the middle-latitude region. Moreover, the receiving station, in comparison to the transmitting station, is situated in the Earth-ionosphere waveguide separation zone, where low-frequency signals are more susceptible to electromagnetic layer disturbances.

The central frequency of low-frequency time-code signals primarily ranges between 40 kHz and 80 kHz, which are radio signals with strong long-range propagation capabilities. Their propagation path includes both ground waves and sky waves. Ground waves propagate along the Earth's surface, while sky waves rely on reflection between the Earth's surface and the ionosphere. As a result, these signals are highly sensitive to changes in the ionospheric electron density and refractive index. When the ionosphere is disturbed, such as by an increase or decrease in electron density, significant changes occur in the propagation path, attenuation characteristics, and signal strength of low-frequency signals. Therefore, low-frequency signals are not only an important means of communication but also provide highly sensitive data support for studying ionospheric disturbances.

The propagation of low-frequency time-code signals is highly dependent on the reflective properties of the ionosphere, and disturbances caused by solar flares often result in signal offset, delay, and attenuation, thereby affecting their reliability and accuracy. Furthermore, high-energy X-ray radiation from solar flares not only directly impacts signal propagation but also induces precursory disturbances in propagation paths and phases through the ionosphere's anticipatory response. In mid- and low-latitude regions, the ionospheric response exhibits unique dynamic characteristics that differ significantly from those observed in polar regions [5–8]. Additionally, the variations in low-frequency time-code signals induced by solar flares offer a novel perspective for ionospheric research. By monitoring and analyzing changes in signal strength, it is possible to indirectly reflect the dynamic processes of electron density in the ionosphere, thereby providing valuable data support for understanding the characteristics of ionospheric disturbances during solar activity.

1.1. Existing Research

Solar flares are generally categorized into different levels based on the intensity of their X-ray flux. This study specifically focuses on C-class flares, which, despite their lower intensity compared to M-class and X-class flares, are more frequent and can have cumulative effects on the ionosphere. These rapid ionospheric variations directly impact communication, navigation systems, and high-frequency radio communications in polar regions [9–12].

López-Urias et al. (2010) demonstrated that the propagation of low-frequency time-code sky waves is strongly dependent on the ionospheric reflection characteristics, meaning that ionospheric disturbances caused by solar flares often lead to issues such as signal offset, delay, and attenuation. These disturbances, in turn, affect the reliability and accuracy of these signals in critical applications [11]. Studies have shown [7–10] that solar flares release high-energy X-ray radiation, which not only directly impacts signal propagation following flare events but may also induce precursor disturbances in signal propagation paths and

phases through the ionosphere's anticipatory response. Nayak et al. (2021) and Huang et al. (2020) pointed out that the ionosphere at mid- and low latitudes exhibits unique electron density variation characteristics during C-class solar flare events [4,13]. Buzás et al. (2019) emphasized that studying how solar flares influence low-frequency time-code signals through ionospheric interactions is crucial for understanding this complex, indirect impact mechanism [6]. In this study, both the transmission station (Shangqiu, approximately 34.45° N latitude) and the reception station (Xi'an, approximately 34.34° N latitude) are located in the mid-latitude region, making them typical cases for analyzing the dynamic characteristics of the mid-latitude ionosphere.

Although considerable progress has been made in investigating the relationship between solar flares, the ionosphere, and low-frequency signal propagation, most research has concentrated on the effects of intense flare events, such as M-class and X-class flares [14–19]. In contrast, the impact of C-class flares, which are weaker but more frequent, on the ionosphere and low-frequency time-code signals has not been sufficiently explored. While the individual effects of these weaker flares may appear small, their frequent occurrence could lead to cumulative effects on ionospheric dynamics and long-term radio communication. However, research on C-class solar flares has largely been confined to case studies, with a notable lack of quantitative analysis regarding the changes in low-frequency time-code signal strength during such events. This study, therefore, aims to offer a new perspective on ionospheric response mechanisms by analyzing the lag time between low-frequency signal strength fluctuations and C-class flare events. Furthermore, the research seeks to assess the potential impact of C-class flares on low-frequency time-code signal propagation, providing scientific evidence to improve communication system stability and enhance resistance to interference. Additionally, by incorporating Granger causality testing, this study further validates and quantifies the causal relationship between C-class solar flares and changes in low-frequency signal strength, thereby offering a foundation for future early-warning and predictive models.

1.2. Research Objectives

The primary objective of this study is to investigate the correlation between low-frequency time-code signal strength and C-class solar flares (XRA). By analyzing lag time and correlation, this study explores the linear and nonlinear relationships between XRA and signal strength across different lag intervals, as well as the disturbance patterns caused by solar flares on signal propagation paths. However, while correlation analysis reveals statistical dependencies between variables, it does not establish causality. Therefore, this study further incorporates Granger causality testing to determine whether changes in XRA can predict variations in low-frequency signal strength. Granger causality testing not only quantifies the temporal precedence of XRA events but also uncovers the deeper influence of solar flare intensity and ionospheric conditions on signal propagation. By integrating correlation analysis with Granger causality testing, this study aims to provide new insights into the mechanisms by which solar flares disturb the ionosphere and offer a theoretical reference for future research on space weather forecasting using low-frequency signals.

2. Data Processing and Analysis Procedure

2.1. Data Sources

In the study of solar storm events, selecting station data with high sensitivity and long-term stability is crucial. For this purpose, this study utilized signal strength data from the Xi'an monitoring station, which records low-frequency time-code signals transmitted from the Shangqiu station. The Xi'an station has been in continuous operation for over two years, and this study specifically selected one year of accumulated signal strength data

following its formal commissioning. Located in the terrestrial wave interference zone of the Shangqiu transmitting station, the Xi'an station provides signal strength data that is particularly valuable for investigating ionospheric response characteristics.

During the daytime, the ionosphere is directly influenced by solar radiation, leading to a significant increase in electron density and more pronounced disturbances. Consequently, the ionosphere exerts a greater impact on the reflection and propagation of long-wave signals during the daytime. In contrast, at night, the Earth's rotation shields the ionospheric region above the receiving station from direct solar radiation, resulting in a substantial decrease in electron density and reduced ionospheric disturbances. Therefore, this study specifically selected solar storm events that occurred during daytime periods at the receiving station to accurately evaluate the impact of solar storms on low-frequency signal strength while minimizing interference from nocturnal ionospheric activity.

Additionally, geomagnetic activity is an important factor influencing the propagation of low-frequency signals, particularly in mid-latitude regions. Enhanced geomagnetic activity can induce severe ionospheric disturbances, significantly altering the signal propagation path and strength. This study utilizes XRA data obtained from NOAA's satellite monitoring systems [20]. Moreover, geomagnetic activity may simultaneously affect both X-ray flux and signal strength, thereby acting as a confounding variable that could obscure the direct impact of solar flares. To address this issue, events coinciding with significant geomagnetic activity (Kp index > 4) were excluded from the analysis to minimize potential interference.

In general, to ensure data reliability and consistency, the following selection criteria were applied in this study: (1) Data Integrity: Only events with complete and continuous data for both X-ray flux and low-frequency signal strength were retained; any events with missing or incomplete data were discarded. (2) Daytime Impact: Only events that occurred during daytime periods at the monitoring station were included to avoid the influence of nocturnal ionospheric activity. (3) Geomagnetic Activity: Events coinciding with significant geomagnetic activity (Kp index > 4) were excluded to reduce the impact of geomagnetic disturbances as a potential confounding variable.

Regarding the input data, this study utilizes a systematically organized dataset to analyze C-class solar flare events, as depicted in Figure 1. The dataset is structured into two primary categories: XRA Data and Signal Strength Data, with each category containing multiple event entries. For each event, the XRA Data and Signal Strength Data are synchronized to the same UTC time period, ensuring consistency and reliability in capturing the ionospheric response to solar activity. The focus of this study is on events recorded during the daytime by the Xi'an monitoring station between May 2023 and June 2024. After applying rigorous selection criteria—such as excluding nighttime events, ensuring data integrity, and filtering out events with Kp index > 4—over 150 valid events were retained for analysis.
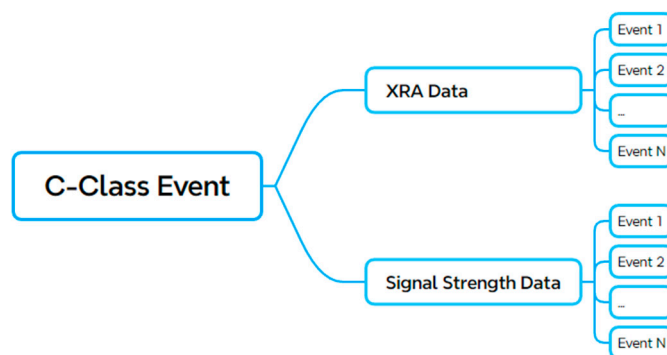

Figure 1. Hierarchical Structure of C-Class Solar Flare Event Dataset.

2.2. Data Processing Methods

To investigate the impact of solar storms on low-frequency signal strength, this study employs the Savitzky-Golay filter [21] to smooth raw signal strength data and extract more accurate trends in signal variation. Compared to other commonly used smoothing methods, such as moving average filters, the Savitzky-Golay filter applies local polynomial fitting to achieve data smoothing. This approach not only effectively reduces high-frequency noise but also maximally preserves the local features and critical characteristics of the signal, such as abrupt changes and peaks. Previous studies have demonstrated that this method exhibits significant advantages in time-series analysis, particularly in retaining data trends while minimizing distortions to lag-dependent features [21–23]. Furthermore, empirical research has verified that Savitzky-Golay filtering does not introduce notable distortions to the key dynamic characteristics analyzed in lag and correlation studies [24,25]. Additionally, this method has proven particularly effective in capturing genuine signal variation trends in high-noise environments and has been widely applied in analyzing dynamic changes caused by solar flares [26,27]. In this study, the filter parameters, including window size and polynomial degree, were carefully optimized to adapt to the complex dynamic relationship between low-frequency time-code signals and X-ray flux (XRA).

2.2.1. Data Correlation and Alignment

To examine the temporal correlation between low-frequency signal strength and XRA (X-ray flux), a cross-correlation analysis method was applied. This approach calculates the correlation between two time series at different time lags, helping to identify the potential time window during which XRA influences signal strength changes. The formula for calculating the cross-correlation function is as follows:

$$R_{xy}(\tau) = \frac{\sum\limits_{t=1}^{N} [x(t) - \overline{x}][y(t+\tau) - \overline{y}]}{\sqrt{\sum\limits_{t=1}^{N} [x(t) - \overline{x}]^2 \sum\limits_{t=1}^{N} [y(t+\tau) - \overline{y}]^2}} \tag{1}$$

where $x(t)$ and $y(t)$ represent the signal strength data and XRA data, respectively; $\overline{x}$ and $\overline{y}$ are the mean values of the corresponding datasets; and τ denotes the lag time, with positive values indicating that XRA changes lead, and negative values indicating that signal strength changes lead.

By calculating the cross-correlation function, the optimal lag time (i.e., the lag value with the highest correlation) between signal strength and X-ray flux (XRA) can be identified. This analysis provides critical insights into the temporal interplay between solar flares and ionospheric dynamics, illustrating how XRA modulates ionospheric reflection properties and subsequently influences the propagation characteristics of low-frequency signals. A positive lag indicates that variations in XRA precede changes in signal strength, implying that an increase in X-ray flux rapidly enhances electron density within the ionosphere. This elevation modifies reflection characteristics, leading to alterations in signal propagation paths and intensity. These findings align with established theories, which posit that solar flares elicit immediate and measurable responses in the ionosphere.

Conversely, a negative lag suggests that changes in signal strength precede variations in XRA, potentially reflecting the influence of complex ionospheric processes not exclusively driven by XRA. Previous studies have indicated that during solar storms, high-energy particle precipitation, such as protons from solar energetic particle (SEP) events, may initiate precursor disturbances in the D-region ionosphere, altering electron density and thus impacting low-frequency signal propagation before significant XRA changes are

detected [8]. This phenomenon may be explained by the faster arrival of energetic particles compared to X-rays, leading to early ionization effects that manifest as signal strength variations [8,10]. As XRA intensifies, these emissions further disrupt ionospheric conditions, potentially amplifying or reversing initial signal trends. Additionally, negative lags may highlight cumulative or secondary effects from localized geomagnetic activity or high-energy particle flux, which act synergistically with XRA to produce complex ionospheric responses [11,17]. These findings underscore the importance of considering multiple contributing factors when interpreting lag dynamics between signal strength and XRA. In this study, the primary focus is on the relationship between XRA and low-frequency time-code signal strength. To minimize the influence of geomagnetic activity as a confounding factor, data from periods with significant geomagnetic disturbances (e.g., Kp > 4) were excluded during preprocessing. Therefore, any observed negative lags are more likely attributable to ionospheric changes driven by XRA and associated solar flare dynamics, rather than the effects of geomagnetic activity.

By systematically analyzing these lag times, this study bridges observed temporal patterns with the underlying physical mechanisms governing ionospheric and signal propagation responses. This integrative approach enhances our understanding of how solar flares, through both direct and indirect pathways, shape the behavior of low-frequency signals, providing a robust framework for investigating space weather phenomena.

2.2.2. Correlation Analysis Between Long-Wave Signals and XRA Data

When investigating the relationship between low-frequency signal strength and X-ray flux (XRA) during solar storms, correlation analysis is a crucial method for uncovering the inherent connection between the two variables. Given that solar storms can cause diverse ionospheric disturbances, which may manifest as signal patterns ranging from linear to nonlinear relationships, the application of multiple correlation metrics is essential for obtaining a comprehensive understanding of the dynamic interactions between long-wave signal strength and XRA. In this study, three correlation indicators were used for a thorough analysis:

(1)　Pearson Correlation Coefficient

The Pearson correlation coefficient is the most widely used metric for quantifying the linear relationship between two variables and is defined as follows:

$$r = \frac{\sum\limits_{i=1}^{N}(x_i - \overline{x})(y_i - \overline{y})}{\sqrt{\sum\limits_{i=1}^{N}(x_i - \overline{x})^2}\sqrt{\sum\limits_{i=1}^{N}(y_i - \overline{y})^2}} \tag{2}$$

where x_i and y_i represent the values of long-wave signal strength and X-ray flux, respectively, $\overline{x}$ and $\overline{y}$ are their mean values. The Pearson correlation coefficient r ranges from [−1, 1], where a value of 1 indicates a perfect positive correlation, −1 indicates a perfect negative correlation, and 0 indicates no linear relationship. In the context of this study, the Pearson coefficient quantifies the degree of linear dependence between X-ray flux (XRA) and low-frequency signal strength. A strong positive or negative r suggests that changes in XRA have a direct and proportional impact on ionospheric electron density, which subsequently alters signal propagation characteristics. This makes Pearson correlation particularly valuable for identifying clear, linear relationships during solar flare events.

(2)　Spearman Rank Correlation Coefficient

The Spearman rank correlation is used to assess the monotonic relationship between two variables and is defined as follows:

$$r_s = 1 - \frac{6\sum d_i^2}{n(n^2 - 1)} \tag{3}$$

where d_i represents the difference in rankings between the two variables, and n is the number of data points. The Spearman correlation is particularly suitable for analyzing nonlinear but monotonic relationships. During solar storms, the relationship between XRA and long-wave signal strength often deviates from linearity, particularly during low-intensity events. As a rank-based metric, the Spearman correlation is well-suited for capturing these intricate nonlinear associations, offering robust insights into ionospheric response patterns under conditions dominated by weak disturbances or elevated noise levels. Its ability to detect subtle yet consistent trends make it particularly advantageous for analyzing complex datasets where linear correlation methods may fail to reveal underlying relationships.

(3)   Kendall Tau Correlation Coefficient

The Kendall Tau coefficient is used to assess the degree of concordance between two variables, and it is defined as follows:

$$\tau = \frac{(N_c - N_d)}{\frac{1}{2}n(n - 1)} \tag{4}$$

where N_c represents the number of concordant pairs and N_d denotes the number of discordant pairs. The Kendall Tau correlation coefficient is a robust and stable measure of association, particularly suited for scenarios involving small sample sizes or datasets with significant variability. Unlike the Pearson correlation coefficient, which primarily assesses linear relationships, Kendall Tau focuses on the consistency of trend changes between variables rather than their absolute values. Additionally, compared to the Spearman correlation coefficient, Kendall Tau provides a more accurate reflection of trend alignment in smaller datasets and is especially effective for analyzing high-noise or dynamically fluctuating data. In this study, the relationship between X-ray flux (XRA) and low-frequency signal strength does not always exhibit linear or instantaneous characteristics but often manifests as cumulative trends that reflect the impact of solar flares on ionospheric disturbances. The rank-based methodology of Kendall Tau is well-suited for capturing these trend consistencies, particularly in identifying the alignment of long-term and short-term trends across different lag intervals. This capability offers a supplementary perspective for understanding the trend-based variations in ionospheric dynamics and low-frequency time-code signal propagation caused by solar flares, addressing the limitations of Pearson and Spearman correlation analyses in capturing complex trends.

In summary, based on the objectives of the study and the characteristics of the data, we consider Spearman's rank correlation coefficient and Kendall's Tau correlation coefficient to be more appropriate statistical methods. This is due to the potential nonlinearity and irregular distribution of the data, which these methods are better equipped to capture. The Pearson correlation coefficient is employed as a supplementary reference, particularly in cases where the data exhibits a linear relationship.

2.2.3. Granger Causality Test

To further investigate the causal drivers of changes in low-frequency signal strength during XRA events, this study introduces the Granger causality test. The Granger causality test is a statistical method used to determine the presence of a causal relationship between time series. In the context of studying the relationship between X-ray flux (XRA) and

low-frequency signal strength during solar storms, this test helps us determine whether changes in XRA can statistically predict variations in long-wave signal strength. This is crucial for understanding the disturbance mechanisms in the ionosphere and the impact of solar storms on low-frequency signal propagation characteristics.

The basic model for the Granger causality test is as follows:

$$Y_i = \alpha_0 + \sum_{i=1}^{P} \alpha_i Y_{t-i} + \sum_{j=1}^{q} \beta_j X_{t-j} + \varepsilon_i \tag{5}$$

In this model, Y_t represents the long-wave signal strength, X_t is the X-ray flux (XRA), and ε_t is the residual. The Granger causality test determines whether X Granger-causes Y by comparing the goodness-of-fit of two models. One model includes only the autoregressive terms of Y, while the other model incorporates lagged values of X. If the inclusion of lagged X significantly improves the model's fit to Y, then X is considered to Granger-cause Y.

In the context of this study, the Granger causality test is used to evaluate whether changes in XRA can significantly explain and predict fluctuations in long-wave signal strength. This approach not only quantifies the time-dependent relationship between the two variables but also reveals potential causal chains. For instance, in the case of a positive lag (i.e., when changes in XRA precede changes in signal strength), a significant test result would suggest that the enhancement of X-ray flux might directly alter the ionospheric electron density, thereby affecting the propagation path of low-frequency signals. The temporal precedence in this relationship is crucial for predicting the effects and response mechanisms of ionospheric disturbances.

On the other hand, if the test shows a significant result in the case of a negative lag (i.e., when signal strength changes precede changes in XRA), it may suggest the existence of a complex ionospheric feedback mechanism. For example, the early arrival of high-energy particle flows may have already disturbed the ionosphere, and changes in XRA could later amplify this effect. This phenomenon implies that XRA is not the sole causal factor but rather an important yet complex variable in the ionospheric disturbance process. In brief, the Granger causality test adds a temporal dimension to our analysis, providing crucial statistical support, particularly in exploring the dynamic influence between solar flares and signal strength.

3. Results and Discussion of Data Analysis

3.1. Case Study of a Single Event

Taking the C2.1-class solar flare event that occurred on 3 May 2023 (local time: 11:39–11:53) as a case study, we performed a qualitative analysis to explore the relationship between low-frequency signal field strength and XRA data. As shown in Figure 2, the variations in field strength and XRA data during this period are presented. In the field strength variation graph (Figure 2, top), the blue curve represents the raw field strength data, while the red curve corresponds to the smoothed data. It is evident that the field strength exhibited a significant upward trend during the solar flare, which likely reflects ionospheric disturbances induced by the flare, leading to enhanced signal propagation strength. Concurrently, the XRA data variation graph (Figure 2, bottom) shows dynamic changes in X-ray flux intensity, displaying a characteristic dip followed by a rise. This pattern aligns with the typical temporal evolution of C-class solar flare events. Based on observations of over 150 similar cases, we hypothesize that variations in XRA data may correlate with trends in field strength.
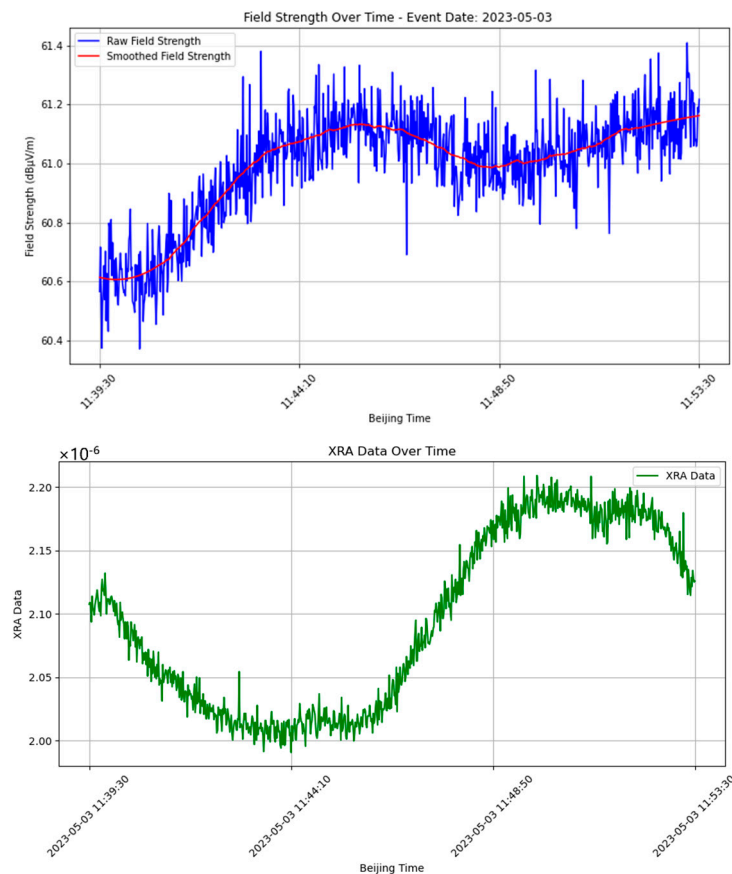
Figure 2. Comparison of Field Strength and XRA Data During a C2.1-Class Event.

As depicted in Figure 3, the cross-spectral density (CSD) between field strength and XRA data is shown as a function of frequency. The results indicate that the two datasets exhibit strong correlations in the low-frequency range (<0.1 Hz), as evidenced by high cross-spectral density values. However, as the frequency increases, the cross-spectral density decreases, suggesting weaker correlations at higher frequencies. The high-density region in the low-frequency range is likely associated with ionospheric electron density changes induced by solar flares. The high-energy X-rays released by solar flares rapidly affect the ionosphere, causing a systemic change in signal propagation paths. Such changes are typically gradual and sustained, predominantly reflected in the low-frequency range. In contrast, the lower density observed in the high-frequency range may be attributed to rapid, localized disturbances, such as instrumental noise or environmental interference.
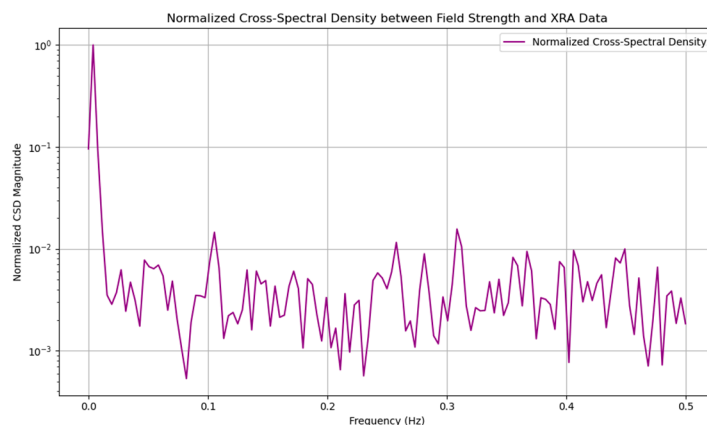

Figure 3. Cross-Spectral Analysis Between Field Strength and XRA Data During a C2.1-Class Event.

Overall, the time-domain signal observations and cross-spectral analysis collectively reveal a potential correlation between field strength and XRA data. Detailed quantitative results and further statistical analysis are presented in Sections 3.2 and 3.3.

3.2. Correlation Analysis Results

Figure 4 presents the statistical histogram of the time lag corresponding to the maximum correlation between the signal strength data and XRA data, based on a sample space of 152 cases. To evaluate the significance of the lag distribution, descriptive statistical metrics were calculated, including the mean lag time (-147.90 s), standard deviation (316.64 s), and skewness (0.50), indicating a slightly right-skewed distribution. Additionally, a Kolmogorov-Smirnov (K-S) test was conducted, comparing the observed lag distribution with a random noise baseline generated using a Gaussian distribution (mean = 0, standard deviation = 5). The choice of 5 s as the standard deviation is supported by studies such as Grubor et al. (2005) and Thomson et al. (2011) [9,10] which identified this range as representative of typical background noise variations in low-frequency signal propagation. The test results (K-S statistic = 0.72, *p*-value = 7.15×10^{-76}, $p < 0.01$) confirm that the lag distribution is significantly different from random noise, supporting the hypothesis that it is driven by ionospheric dynamics rather than stochastic fluctuations.
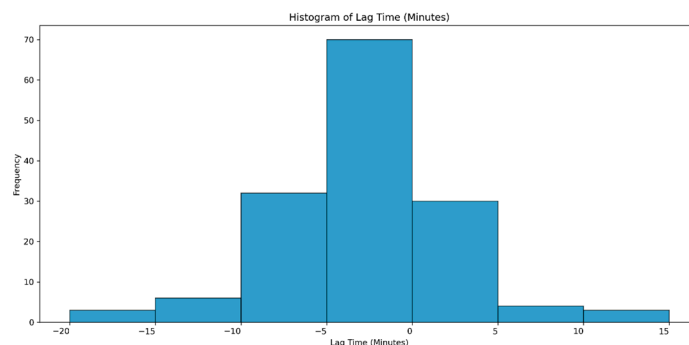

Figure 4. Histogram of Lag Time (Minutes).

From the figure, it is evident that the most probable time lag occurs within the interval of -5 to 0 min, where the signal strength changes precede the C-class XRA changes. This finding aligns with the ionospheric pre-disturbance phenomenon reported in previous studies. For example, Kumar et al. (2017) pointed out that in weaker solar flare events, background disturbances in the ionosphere can cause fluctuations in signal strength several minutes before the onset of the flare event [7]. This may be due to early signals from high-energy particle flows or solar radiation fluctuations, which, although not directly observed, have already begun to influence the propagation path of low-frequency signals.

The next most probable time lag occurs between 0 and 5 min, indicating that the signal strength was further disturbed after the XRA event began. This is consistent with the findings of Grubor et al. (2005), who observed that C-class solar flare events significantly increased the electron density in the ionospheric D-layer within minutes, thereby altering the propagation path of low-frequency signals [9].

A relatively earlier negative time lag (from -10 to -5 min) accounted for 21.48% of occurrences, suggesting that significant changes in signal strength might have already been triggered by precursor disturbances before the C-class XRA event. These disturbances are likely associated with the instability of the ionosphere in the polar regions or the early stages of high-energy solar particle activity. Such early responses were also noted in the study by Clilverd et al. (2001), which indicated that even low-level solar flare events could affect the propagation of low-frequency time-code signals in the polar regions due to precursor disturbances [8].

The significance of time lags longer than 5 to 10 min, or beyond, shows a notable decline. This phenomenon is consistent with the findings of Thomson et al. (2011), who noted that the impact of C-class events on the ionosphere is typically short-lived, usually recovering within a few minutes [10].

3.3. Correlation Coefficient Analysis and Its Relationship with Low-Frequency Signal Response

In calculating the correlation coefficients, this study first aligns the low-frequency signal strength with the XRA data based on the lag time obtained from the analysis in Section 2.2, ensuring optimal correlation alignment. The Pearson, Spearman, and Kendall Tau correlation coefficients are then computed. This approach ensures that the correlation coefficients accurately reflect the relationship between the XRA and signal strength variations after correcting for lag time. Lag time alignment not only removes the interference caused by temporal misalignment between the signals but also enhances the accuracy of the correlation analysis. This method is widely used in the literature to address the issue of underestimating correlation in dynamic systems due to signal delays. For instance, Clilverd et al. (2001) demonstrated that lag alignment improves the capture of the relationship between VLF signals in polar regions and solar activity [8], while Kumar et al. (2017) highlighted that lag correction aids in more accurately quantifying the impact of solar flares on ionospheric disturbances [7].

Figure 5 shows the distribution of lag times and the three correlation coefficients for each sample, while Table 1 provides the statistical results of the three correlation coefficients across different time intervals. The selection of a 5-min interval for lag segmentation is based primarily on the time-scale characteristics of ionospheric disturbances caused by solar flares and the anomaly detection features of signal receiving terminals. Grubor et al. (2005) pointed out that C-class solar flares typically induce significant changes in ionospheric electron density within a few minutes [9]. Thomson et al. (2011) further emphasized that a 5-min interval effectively captures dynamic changes within this time scale while maintaining a balance between analytical precision and interpretability, avoiding the amplification of random noise from overly small segments or the loss of subtle variations with excessively large segments [10]. Additionally, Mitra (1974) noted that significant fluctuations within a 5-min period are often regarded as anomalous signals from the perspective of signal receiving terminals, potentially reflecting rapid disturbances caused by solar activity [12]. From the figure, it is evident that in the lag intervals $(-5, 0)$ and $(0, 5)$, the average Pearson correlation coefficient is significantly positive, indicating a strong linear relationship between XRA and signal strength during these periods. In contrast, negative correlations are observed in the earlier negative lag intervals. For example, for a sample with a lag of -144 s (approximately -2.4 min), the Pearson correlation coefficient is 0.75, which lies within the high positive correlation range $(-5, 0)$, demonstrating that near the peak of the flare, XRA is strongly linearly associated with changes in signal strength. However, it is important to note that this is just one sample case, and such a high correlation may not be representative of the overall trend. These results suggest that the most significant positive correlation between XRA and signal strength occurs within the lag intervals $(-5, 0)$ and $(0, 5)$. This indicates that during C-class flare events, an increase in XRA directly causes changes in the ionospheric electron density, which in turn alters the propagation characteristics of low-frequency skywave signals. The high linear correlation observed during this period underscores the significant direct impact of C-class flares on low-frequency signals.
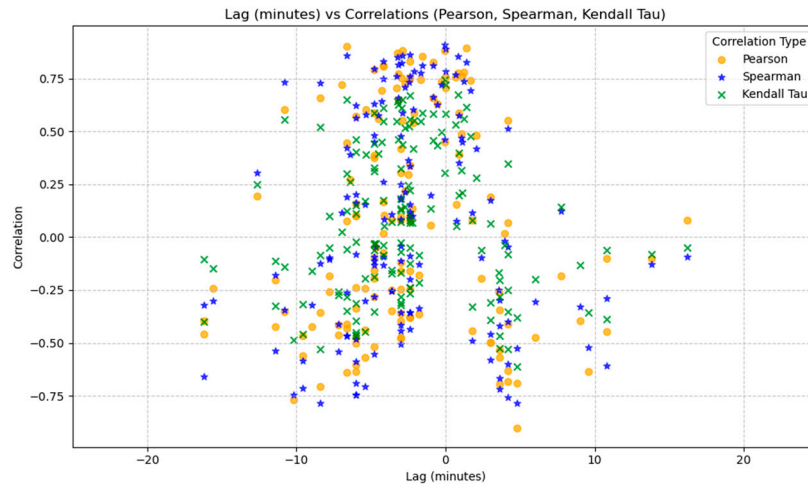
Figure 5. Distribution of the Three Correlation Coefficients with Lag Time.

Table 1. Comparison of the Distribution of the Three Correlation Coefficients Across Different Lag Intervals.

Lag Bin (Minutes)	Pearson Avg	Spearman Avg	Kendall Tau Avg
$(-20, -15)$	-0.15	-0.12	-0.08
$(-15, -10)$	-0.20	-0.19	-0.12
$(-10, -5)$	0.18	0.23	0.15
$(-5, 0)$	0.45	0.52	0.38
$(0, 5)$	0.38	0.42	0.31
$(5, 10)$	0.20	0.19	0.14
$(10, 15)$	-0.05	-0.02	-0.01
$(15, 20)$	-0.12	-0.11	-0.06

The Spearman correlation coefficient reaches its peak value in the lag interval $(-5, 0)$, highlighting a highly significant monotonic relationship between signal strength and XRA. For example, for a sample with a lag of -174 s (approximately -2.9 min), the Spearman correlation coefficient is 0.86, indicating a high degree of monotonic consistency between signal strength and XRA changes just before the flare peak. The Spearman results further reinforce the rapid response of the ionosphere to XRA, especially in the lag interval $(-5, 0)$. This strong monotonicity suggests that even in the presence of strong noise or nonlinear effects, signal strength remains a reliable indicator of XRA's changing trend. The Kendall Tau coefficient reaches a significant positive value in the lag interval $(-5, 0)$, with a slightly lower value in the $(0, 5)$ interval, suggesting that the trend of signal strength changes aligns closely with XRA. Moreover, in earlier negative lag intervals (e.g., -15, -10), the trend changes in signal strength may serve as a precursor to an upcoming flare event.

In summary, the combined results of the three correlation coefficients indicate that, within the key lag intervals of $(-5, 0)$ and $(0, 5)$, the high positive correlation between XRA and signal strength reveals a direct and rapid impact of C-class solar flares on ionospheric reflection characteristics. This correlation supports the hypothesis that solar storms cause ionospheric disturbances, with the positive correlation persisting even after the event (5 to 10 min). This suggests that the high-energy radiation from the flare has a lasting effect on the ionosphere, resulting in continuous changes in signal propagation paths and signal strength. The early negative correlation observed in the lag interval $(-20, -10)$ suggests that C-class flares may act as a warning signal for ionospheric disturbances, with signal strength being affected even before the flare reaches C-class intensity.

Furthermore, from the perspective of the three correlation coefficients and their relation to the geomagnetic storm levels, as illustrated in Figure 6, the Pearson Correlation shows a

significant increase from 0.38 for C1–C3 to 0.58 for C7–C9. This indicates that as the flare intensity increases, the linear correlation between XRA and signal strength strengthens. This suggests that more intense solar flares likely have a more pronounced direct impact on ionospheric disturbances and the propagation of low-frequency signals. The Spearman Correlation (monotonic relationship) rises from 0.33 to 0.64, signifying that during stronger flare events, even nonlinear trends exhibit greater consistency. Similarly, the Kendall Tau Correlation increases from 0.27 to 0.53, further confirming that as the flare level intensifies, the stability of the relative relationships between data points improves.
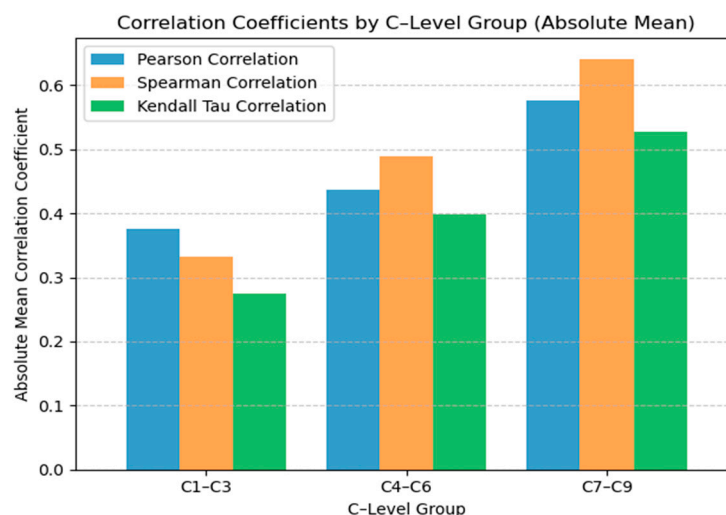

Figure 6. Distribution Statistics of Solar Storms of Different Intensity Levels and Correlation Coefficients.

3.4. Granger Causality Test Analysis

In Section 3.2, the correlation analysis revealed both linear and nonlinear relationships between C-class XRA events and low-frequency signal strength. However, correlation does not imply causality. To further investigate whether XRA events are the causal drivers of changes in low-frequency signal strength, we applied the Granger causality test. The Granger causality test is a statistical method based on the predictive capability of time series data, used to assess whether the historical values of one variable can significantly predict the future values of another [7]. In this study, this approach allows us to assess whether changes in XRA are causally related to fluctuations in signal strength over time.

The results of the Granger causality test are expressed in terms of *p*-values. Smaller *p*-values indicate a stronger statistical significance of the causal relationship. Typically, a *p*-value of less than 0.05 is considered to indicate a significant Granger causal relationship. For example, in the data used in this study, a sample with a lag of 50 s corresponds to a Granger *p*-value of 0.0007, suggesting that even with a relatively short lag time, the influence of XRA on signal strength remains statistically significant. This study investigates the causality between signal strength and XRA data in 5-min intervals, specifically analyzing the differences in causality before and after solar storm events. The average percentage of *p*-values below 0.05 for each time interval was calculated as a measure of significance, used to evaluate the strength of the causal relationship in each period.

The results of the significance evaluation show that the *p*-values in the lag intervals of $(-5, 0)$ and $(0, 5)$ minutes are notably lower, indicating the strongest Granger causality between XRA and signal strength during these periods, as shown in Figure 7. In the negative lag intervals (-20 to 0 min), the significance level increases from 13.33% to 60%, suggesting that when changes in low-frequency signal strength precede changes in X-ray flux, the Granger causality gradually intensifies. This phenomenon supports the hypothesis that the ionospheric response to low-frequency signals may occur before changes in X-ray

flux. In the intervals of $[-10, -5)$ and $[-5, 0)$, the significance levels are 41.25% and 60%, respectively. These elevated significance values suggest that variations in low-frequency signal strength could represent an early response to an impending XRA event. These findings support the earlier argument regarding the sensitivity of low-frequency signal strength to early ionospheric disturbances. Even before the solar storm reaches C-class levels, changes in signal strength can already detect ionospheric ionization effects induced by X-ray radiation. However, while the significance levels of 41.25% and 60% suggest some degree of correlation, they are not exceptionally strong. It is crucial to emphasize that Granger causality identifies statistical causality but does not confirm physical causality. This distinction highlights that while these results point to a potential relationship, they should not be interpreted as conclusive evidence of a direct physical link. Therefore, these findings should be viewed as a basis for further exploration, rather than definitive proof.
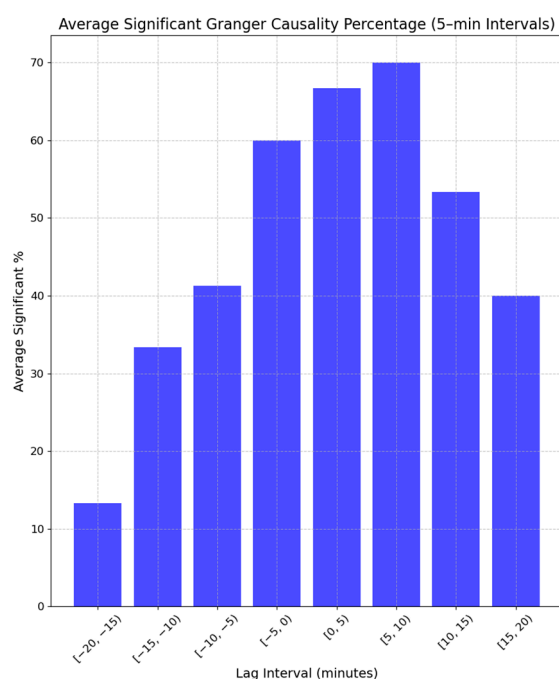

Figure 7. Average Significant Granger Causality Percentage.

For the positive lag intervals (0 to 20 min), the significance in the intervals of $[0, 5)$ and $[5, 10)$ is 66.67% and 70%, respectively, marking the periods with the highest significance. This indicates a strong Granger causal relationship between the increase in X-rays and the subsequent changes in low-frequency signal strength. After 10 min, the significance starts to decline, but the correlation remains relatively high (e.g., 53.33% in the interval $[10, 15)$). This suggests that the impact of XRA events can still be observed for a period after their occurrence.

By restricting the analysis to events with Kp < 4, the influence of geomagnetic activity as a confounding variable is minimized, ensuring that the observed relationships between signal strength changes and XRA are predominantly driven by ionospheric dynamics. In the negative lag intervals, early changes in signal strength are observed as an ionospheric pre-response to the impending XRA disturbance, demonstrating the predictive potential of these signal strength variations. In the positive lag intervals, the significant influence of XRA on low-frequency signal strength is concentrated in the 0–10 min period following the event, demonstrating the immediate impact of the X-ray event on the ionosphere. This analysis confirms that C-class XRA events have a considerable effect on low-frequency signals, with this effect exhibiting both a time delay and predictive potential.

4. Conclusions

This study explores the impact of C-class solar flares (XRA) on the ionosphere and low-frequency signal propagation by analyzing the lag time, correlation coefficients, and Granger causality between low-frequency signal strength and XRA data. The main conclusions are as follows:

(1) Correlation Analysis: The results indicate that within the lag intervals of $(-5, 0)$ and $(0, 5)$ minutes, the low-frequency signal strength and XRA show the highest correlation, suggesting a rapid ionospheric response to XRA disturbances. Significant changes in signal strength are observed even before the peak of the flare. The negative lag intervals $(-10, -5)$ and earlier periods support the theory of ionospheric pre-response, indicating that changes in signal strength may precede XRA events, which serves as an early warning of impending solar flares. In the positive lag interval $(0, 10)$, the signal strength closely follows the increase in XRA, reflecting the sustained impact of XRA on the ionosphere.

(2) Correlation Coefficient Analysis: As the intensity of C-class solar flares increases (from C1–C3 to C7–C9), the Pearson correlation coefficient increases from 0.38 to 0.58, demonstrating a stronger linear effect of higher intensity flares on signal propagation. Both the Spearman and Kendall Tau coefficients also rise with increasing flare intensity, indicating a stronger relationship between signal strength and XRA in terms of non-linear trends and consistency. These findings highlight that low-frequency signal strength is highly sensitive to XRA disturbances, supporting the hypothesis that C-class solar flares have a direct impact on the ionosphere.

(3) Granger Causality Test: The Granger causality test further confirms the causal relationship between signal strength and XRA data. The significance levels in the lag intervals $(-5, 0)$ and $(0, 5)$ are the highest, reaching 60% and 66.67%, respectively, indicating that XRA has the most significant causal impact on signal strength during these periods. In the negative lag interval $(-10, -5)$, the significance level is 41.25%, supporting the idea that low-frequency signal strength responds predictively to impending XRA events. In the positive lag interval $(0, 10)$, the significance reaches 70%, indicating that the impact of XRA on signal strength persists for several minutes after the flare.

Through a multi-faceted analysis of lag time, correlation coefficients, and Granger causality, this study confirms the significant influence of C-class solar flare events on low-frequency signal propagation in the ionosphere and the Earth-ionosphere wave interference region. This impact is not only characterized by the ionosphere's rapid response to XRA events and its early warning capabilities but also by the lasting disturbance effects following the event. Despite the relatively low energy of C-class solar flares, their impact on the ionosphere and low-frequency signals is immediate, sustained, and predictive. These findings reveal the correlation between C-class solar flares and low-frequency time-code signal strength, providing theoretical support for the application of low-frequency signals in space weather monitoring and early warning systems. However, it is crucial to emphasize that these results do not establish a strong causal relationship between variations in low-frequency signal strength and C-class solar flare events, as statistical causality, such as that identified through Granger causality, does not confirm the underlying physical causality. The practical application of these results requires further validation in real-world scenarios, including the incorporation of long-term observational data from additional fixed stations to enhance the predictive accuracy and applicability of the proposed methods. Building on this foundation, future work can proceed in three directions: first, by integrating monitoring data from more fixed stations to further refine the statistical analysis; second, by extending the study to include M-class and X-class solar flares; and third, by incorporating

additional statistical methods to provide a more comprehensive comparison and strengthen the robustness of the findings. This would allow for an exploration of the relationship between flare intensity and ionospheric dynamics, as well as the propagation characteristics of low-frequency signals, thereby verifying the applicability of the observed patterns under higher-intensity flares.

Institutional Review Board Statement: This study does not involve ethical approval.

Informed Consent Statement: This study does not involve human subjects.

Data Availability Statement: The data sets analyzed are available from the corresponding author upon reasonable request.

Conflicts of Interest: The authors declare no conflicts of interest.

References

1. Hayes, L.A.; O'Hara OS, D.; Murray, S.A.; Gallagher, P.T. Solar flare effects on the earth's lower ionosphere. *Sol. Phys.* **2021**, *296*, 157. [CrossRef]
2. Nishimoto, S.; Watanabe, K.; Kawai, T.; Imada, S.; Kawate, T. Validation of computed extreme ultraviolet emission spectra during solar flares. *Earth Planets Space* **2021**, *73*, 79. [CrossRef]
3. Liu, L.B.; Wan, W.X.; Chen, Y.D.; Le, H. Solar activity effects of the ionosphere: A brief review. *Chin. Sci. Bull.* **2011**, *56*, 1202–1211. [CrossRef]
4. Nayak, C.; Yiğit, E. GPS-TEC observation of gravity waves generated in the ionosphere during 21 August 2017 total solar eclipse. *J. Geophys. Res. Space Phys.* **2018**, *123*, 725–738. [CrossRef]
5. López-Urias, C.; Vazquez-Becerra, G.E.; Nayak, K.; López-Montes, R. Analysis of ionospheric disturbances during x-class solar flares (2021–2022) using GNSS data and wavelet analysis. *Remote Sens.* **2023**, *15*, 4626. [CrossRef]
6. Buzás, A.; Kouba, D.; Mielich, J.; Burešová, D.; Mošna, Z.; Koucká Knížová, P.; Barta, V. Investigating the effect of large solar flares on the ionosphere based on novel Digisonde data comparing three different methods. *Front. Astron. Space Sci.* **2023**, *10*, 1201625. [CrossRef]
7. Kumar, A.; Kumar, S. Solar flare effects on D-region ionosphere using VLF measurements during low-and high-solar activity phases of solar cycle 24. *Earth Planets Space* **2018**, *70*, 29. [CrossRef]
8. Clilverd, M.A.; Thomson, N.R.; Rodger, C.J. Sunrise effects on VLF signals propagating over a long north-south path. *Radio Sci.* **1999**, *34*, 939–948. [CrossRef]
9. Grubor, D.; Šulić, D.; Žigman, V. Influence of solar X-ray flares on the Earth-ionosphere waveguide. *Serbian Astron. J.* **2005**, *171*, 29–35. [CrossRef]
10. Thomson, N.R.; Clilverd, M.A. Solar flare induced ionospheric D-region enhancements from VLF amplitude observations. *J. Atmos. Sol.-Terr. Phys.* **2001**, *63*, 1729–1737. [CrossRef]
11. Hargreaves, J.K. *The Solar-Terrestrial Environment: An Introduction to Geospace-the Science of the Terrestrial Upper Atmosphere, Ionosphere, and Magnetosphere*; Cambridge University Press: Cambridge, UK, 1992.
12. Mitra, A.P. *Ionospheric Effects of Solar Flares*; D. Reidel Publishing Company: Boston, MA, USA, 1974.
13. Kumar, A.; Kumar, S. Space weather effects on the low latitude D-region ionosphere during solar minimum. *Earth Planets Space* **2014**, *66*, 76. [CrossRef]
14. McRae, W.M.; Thomson, N.R. Solar flare induced ionospheric D-region enhancements from VLF phase and amplitude observations. *J. Atmos. Sol.-Terr. Phys.* **2004**, *66*, 77–87. [CrossRef]
15. Deshpande, S.D.; Subrahmanyam, C.V.; Mitra, A.P. Ionospheric effects of solar flares—I. The statistical relationship between X-ray flares and SID's. *J. Atmos. Terr. Phys.* **1972**, *34*, 211–227. [CrossRef]
16. Žigman, V.; Grubor, D.; Šulić, D. D-region electron density evaluated from VLF amplitude time delay during X-ray solar flares. *J. Atmos. Sol.-Terr. Phys.* **2007**, *69*, 775–792. [CrossRef]

17. Thomson, N.R.; Rodger, C.J.; Clilverd, M.A. Large solar flares and their ionospheric D region enhancements. *J. Geophys. Res. Space Phys.* **2005**, *110*. [CrossRef]

18. Rozhnoi, A.; Solovieva, M.; Fedun, V.; Gallagher, P.; McCauley, J.; Boudjada, M.Y.; Shelyag, S.; Eichelberger, H.U. Strong influence of solar X-ray flares on low-frequency electromagnetic signals in middle latitudes. *Ann. Geophys.* **2019**, *37*, 843–850. [CrossRef]

19. Zolesi, B.; Cander, L.R. *Ionospheric Prediction and Forecasting*; Springer: Berlin/Heidelberg, Germany, 2014.

20. NOAA. Available online: https://www.ngdc.noaa.gov/stp/satellite/goes-r.html (accessed on 1 July 2024).

21. Savitzky, A.; Golay, M.J.E. Smoothing and differentiation of data by simplified least squares procedures. *Anal. Chem.* **1964**, *36*, 1627–1639. [CrossRef]

22. Brockwell, P.J.; Davis, R.A. *Introduction to Time Series and Forecasting*; Springer: New York, NY, USA, 2002.

23. Gorry, P.A. General least-squares smoothing and differentiation by the convolution (Savitzky-Golay) method. *Anal. Chem.* **1990**, *62*, 570–573. [CrossRef]

24. Press, W.H. *Numerical Recipes: The Art of Scientific Computing*, 3rd ed.; Cambridge University Press: Cambridge, UK, 2007.

25. Schafer, R.W. What is a savitzky-golay filter? *IEEE Signal Process. Mag.* **2011**, *28*, 111–117. [CrossRef]

26. Chen, J.; Jönsson, P.; Tamura, M.; Gu, Z.; Matsushita, B.; Eklundh, L. A simple method for reconstructing a high-quality NDVI time-series data set based on the Savitzky–Golay filter. *Remote Sens. Environ.* **2004**, *91*, 332–344. [CrossRef]

27. Dombi, J.; Dineva, A. Adaptive Savitzky-Golay filtering and its applications. *Int. J. Adv. Intell. Paradig.* **2020**, *16*, 145–156. [CrossRef]